Journal of the Korean Physical Society, Vol. 39, No. 2, August 2001, pp. 271∼279

Time-Dependent Global Modeling of Pulse-Power-Modulated Low Pressure Oxygen Plasmas

Hyun Jin YOON and Tae Hun CHUNG*

Department of Physics, Dong-A University, Pusan 604-714

(Received 12 December 2000)

A time-dependent global model, which consists of energy and particle balance equations, is formulated for a pulse-power-modulated low pressure oxygen discharge plasma. The time evolution of the electron temperature and the plasma density are calculated. Also, the time-resolved charged-particle density and flux are obtained by changing the duty ratio, the modulation frequency, the pressure, and the input power. The effects of pressure and power are checked with the scaling relations derived based on a global balance. The peak negative-ion density in the afterglow increases with the modulation frequency and the input power, decreases with the duty ratio, and shows a maximum with pressure.

I. INTRODUCTION

The use of pulse-power-modulated plasmas is beneficial for a variety of plasma processing applications [1]. If the modulation frequency and the duty ratio are varied, pulsed plasmas provide additional tools in plasma processing. With the aid of pulse-power modulation, the discharge chemistry can be altered to obtain high anisotropy, selectivity, and elimination of microloading during etching [2] and to obtain a higher deposition rate and better quality of thin films when using plasma-enhanced chemical-vapor deposition [3]. Pulsed plasmas have also been used for the suppression of dust particles [4] and for negative-ion sources [5].

Several studies of pulsed plasmas have been reported. These include experimental works using quadrupole mass spectroscopy [6], optical emission spectroscopy [7,8], microwave interferometry [9], and Langmuir probe measurements [10,11]. Among earlier studies, one by Ashida *et al.* [12] analyzed a time-modulated argon discharge by using a spatially averaged model. Spatially averaged global models have also been developed for various operating regions of rf discharge plasmas [13–17] and have been used to study continuous wave (cw) discharges in chlorine [13] and oxygen [14,18] and pulsed discharges in chlorine [16,19,20], SF_6 [21], and CF_4 [19]. Lymberopoulos *et al.* [22] developed a one-dimensional fluid model to investigate the spatiotemporal dynamics of pulsed power inductively coupled argon plasmas. Midha *et al.* [23] did a computational study on pulsed chlorine plasmas by varying control parameters. Boswell and Vendor *et al.* [24,25] developed a particle-in-cell model with non-periodic boundary conditions to simulate pulsed electropositive and electronegative plasmas. Mostaghimi *et al.* [26] developed a two-dimensional model to study the response of inductively coupled plasmas in an argon-hydrogen mixture to a sudden change in its active power under atmospheric pressure conditions.

Plasmas of electronegative gases have drawn interest in connection with pulse-power modulation because the negative ions can be extracted from the decaying afterglow. Especially, oxygen plasmas have found numerous applications in plasma processing, such as reactive sputtering, dry etching of polymers, oxidation, and resist removal of semiconductors. Recently, Panda *et al.* [27] discussed the effect of metastable oxygen molecules in pulsed oxygen plasmas.

In this article, a time-dependent global model is used to analyze a time-modulated oxygen discharge. The characteristics of the plasma parameters as functions of the duty ratio, the modulation frequency, the pressure, and the input power are discussed. We will focus on time-resolved plasma properties of pulse-modulated oxygen plasmas generated by high-density plasma sources. Especially, the effects of the pressure and the power are examined in comparison with the scaling formulas derived based on the global balance equations.

This paper is organized as follows: In Section II, a physical model and basic equations are presented. Some discussion of the scaling laws based on the physical model follows in Section III. Section IV presents the results of calculations and discussions. In section V, conclusions are summarized.

*E-mail: thchung@plasma.donga.ac.kr

II. MODEL EQUATIONS

The reactions considered in this model and the rate constants [28] are

$$e + O_2 \rightarrow O_2{}^+ + 2e \text{ (Ionization 2) } \left\{K_{iz2} = 9 \times 10^{-16} T_e^2 \exp(-12.6/T_e)\right\} \quad (1)$$
$$e + O_2 \rightarrow O^- + O \text{ (Dissociative attachment) } \left\{K_{att} = 8.8 \times 10^{-17} \exp(-4.4/T_e)\right\} \quad (2)$$
$$O_2{}^+ + O^- \rightarrow O_2 + O \text{ (Recombination 2) } \left\{K_{rec2} = 1.5 \times 10^{-13} (300/T_g)^{0.5}\right\} \quad (3)$$
$$O^- + O^+ \rightarrow 2O \text{ (Recombination 1) } \left\{K_{rec1} = 2.5 \times 10^{-13} (300/T_g)^{0.5}\right\} \quad (4)$$
$$e + O^- \rightarrow O + 2e \text{ (Detachment) } \left\{K_{det} = 2 \times 10^{-13} \exp(-5.5/T_e)\right\} \quad (5)$$
$$e + O_2 \rightarrow O^- + O^+ + e \text{ (Pair Production) } \left\{K_{pair} = 7.1 \times 10^{-17} {T_e}^{0.5} \exp(-17/T_e)\right\} \quad (6)$$
$$e + O_2 \rightarrow O + O^+ + 2e \text{ (Dissociative Ionization) } \left\{K_{disiz} = 5.3 \times 10^{-16} {T_e}^{0.9} \exp(-20/T_e)\right\} \quad (7)$$
$$e + O \rightarrow O^+ + 2e \text{ (Ionization 1) } \left\{K_{iz1} = 9 \times 10^{-15} {T_e}^{0.7} \exp(-13.6/T_e)\right\} \quad (8)$$
$$e + O_2 \rightarrow 2O + e \text{ (Dissociation) } \left\{K_{diss} = 4.2 \times 10^{-15} \exp(-5.6/T_e)\right\} \quad (9)$$
$$O^+ \rightarrow O \text{ (Wall recombination)} \quad (10)$$
$$O_2{}^+ \rightarrow O_2 \text{ (Wall recombination)} \quad (11)$$
$$O + O \rightarrow O_2 \text{ (Wall recombination).} \quad (12)$$

Since the energy levels of the metastable oxygen molecule and atom are typically low (*e.g.*, 1 eV), their contributions via stepwise ionization are quite low. Therefore, the effect of metastable species are neglected for the parameter region we examine [14]. In constructing a global (spatially averaged) model, we assume that the spatial profiles of the charged and the neutral particles are flat with their average values and that the charged particles have very small sheath regions.

The densities of neutral O atoms, neutral O_2 molecules, $O^+, {O_2}^+$, and O^-, and the electron temperature are taken into account as independent variables. From the reactions above, the rate equations for the spatially averaged charged particle densities (the symbol [ ] are used) are written as

$$\frac{\mathrm{d}[{O_2}^+]}{\mathrm{dt}} = K_{iz2}[\mathrm{O_2}][\mathrm{e}] - K_{rec2}[{O_2}^+][O^-] - {O_2}^+_{Loss}[{O_2}^+] - \frac{S_p}{V}[{O_2}^+], \quad (13)$$

$$\frac{\mathrm{d}[O^+]}{\mathrm{dt}} = K_{pair}[\mathrm{O_2}][\mathrm{e}] + K_{disiz}[\mathrm{O_2}][\mathrm{e}] + K_{iz1}[\mathrm{O}][\mathrm{e}] - K_{rec1}[O^-][O^+] - O^+_{Loss}[O^+] - \frac{S_p}{V}[O^+]. \quad (14)$$

Particle fluxes of positive ions, electrons, and negative ions are written as

$$\Gamma_+ = \frac{V}{A}\frac{1}{d_{eff}}([O^+]u_{\mathrm{B},O^+} + [{O_2}^+]u_{\mathrm{B},{O_2}^+}),$$

$$\Gamma_{\mathrm{e}} = \frac{1}{4}u_{O^-}\frac{V}{A}\frac{1}{d_{eff}}\frac{1}{1+\alpha}([O^+] + [{O_2}^+])exp\left(\frac{\Phi}{T_{\mathrm{e}}}\right) \quad (\mathrm{m}^{-2}s^{-1}),$$
$$\Gamma_{O^-} = \frac{1}{4}u_{\mathrm{e}}\frac{V}{A}\frac{1}{d_{eff}}\frac{\alpha}{1+\alpha}([O^+] + [{O_2}^+])exp\left(\frac{\Phi}{T_{\mathrm{e}}}\right), \quad (15)$$

where $u_{\mathrm{e}} = \left(\frac{8eT_{\mathrm{e}}}{\pi m_e}\right)^{\frac{1}{2}}$, $u_{O^-} = \left(\frac{8eT_{\mathrm{i}}}{\pi m_{O^-}}\right)^{\frac{1}{2}}$, $\alpha = \frac{[O^-]}{[e]}$, and Φ is the plasma potential. T_e and T_i are the electron and ion temperatures, m_e and m_{O^-} are the electron and ion masses, respectively. $A = 2\pi R^2 + 2\pi RL, V = \pi R^2 L$, and the effective system length is

$$d_{eff} = \frac{RL}{2(Rh_{\mathrm{L}} + Lh_{\mathrm{R}})}. \quad (16)$$

Here, h_{L} and h_{R} are the ratios of the density at the sheath edge to that in the bulk for the axial and the radial directions respectively, and are given from low-pressure diffusion theory as

$$h_{\mathrm{L}} = \frac{0.86(1+2\alpha/\gamma)}{1+\alpha} \times \left[3 + \frac{L}{2\lambda_i} + \left(\frac{0.86Lu_{BO_2^+}}{\pi D_{a+}}\right)^2\right]^{-\frac{1}{2}}, \quad (17)$$

$$h_{\mathrm{R}} = \frac{0.8(1+3\alpha/\gamma)}{1+\alpha} \times \left[4 + \frac{R}{\lambda_i} + \left(\frac{0.8Ru_{BO_2^+}}{2.405J_1(2.405)D_{a+}}\right)^2\right]^{-\frac{1}{2}}, \quad (18)$$

where $\gamma = T_e / T_i$, λ_i is the ion mean-free path, and u_{BO^+} and $u_{BO_2^+}$ are the Bohm velocities of the oxygen atoms and molecules, respectively.

The plasma potential is calculated by assuming the flux conservation

$$\Gamma_+ = \Gamma_e + \Gamma_{O^-}. \quad (19)$$

The negative-ion density balance is written as

$$\frac{d[O^-]}{dt} = K_{att}[O_2][e] - K_{rec2}[O_2^+][O^-] + K_{pair}[O_2][e] - \frac{1}{4}u_{O^-}\frac{1}{d_{eff}}\frac{\alpha}{1+\alpha}([O^+]+[O_2^+])exp\left(\frac{\Phi}{T_e}\right) - K_{det}[O^-][e] - K_{rec1}[O^-][O^+]. \quad (20)$$

The balance of electrons is given in the model as

$$[e] = [O_2^+] + [O^+] - [O^-]. \quad (21)$$

The particle balances for the neutral species are written as

$$\frac{d[O]}{dt} = K_{att}[O_2][e] + K_{rec2}[O_2^+][O^-] - O_{Loss}[O] + O^+_{Loss}[O^+] + 2K_{diss}[O_2][e] + K_{disiz}[O_2][e] + K_{det}[O^-][e] - K_{iz1}[O][e] + 2K_{rec1}[O^-][O^+] - \frac{S_p}{V}[O], \quad (22)$$

$$\frac{d[O_2]}{dt} = \frac{Q_{fs}}{V} - (K_{iz2} + K_{att} + K_{diss} + K_{pair} + K_{disiz})[O_2][e] + K_{rec2}[O_2^+][O^-] + O_2^+_{Loss}[O_2^+] + \frac{1}{2}O_{Loss}[O] - \frac{S_p}{V}[O_2]. \quad (23)$$

Finally the wall loss rates for neutral atoms and charged ions are modeled as

$$O_{Loss} = \gamma_{rec}\frac{v_{th}A}{4V}, \quad O^+_{Loss} = \frac{u_{O^+}}{d_{eff}}, \quad O_2^+_{Loss} = \frac{u_{O_2^+}}{d_{eff}}, \quad (24)$$

where γ_{rec} is the surface recombination coefficient and v_{th} is the thermal velocity of the neutral atom.

The energy balance equation can be written as

$$\frac{d\left(\frac{3}{2}[e]T_e\right)}{dt} = \frac{P_{abs}}{V} - \varepsilon_{c2}K_{iz2}[O_2][e] - \varepsilon_{c1}K_{iz1}[O][e] - (K_{diss}\varepsilon_{diss} + K_{pair}\varepsilon_{pair} + K_{disiz}\varepsilon_{disiz})[e][O_2] - \frac{A}{V}\left[\left(|\Phi| + \frac{T_e}{2}\right)\Gamma_+ + 2T_e\,\Gamma_e + 2T_i\,\Gamma_-\right]. \quad (25)$$

The collisional energy loss can be expressed as

$$K_{iz2}\varepsilon_{c2} = K_{iz2}\varepsilon_{iz2} + \sum K_{exc2}\varepsilon_{exc2} + K_{el2}\varepsilon_{el2}, \quad (26)$$

$$K_{iz1}\varepsilon_{c1} = K_{iz1}\varepsilon_{iz1} + \sum K_{exc1}\varepsilon_{exc1} + K_{el1}\varepsilon_{el1}, \quad (27)$$

where the ε_j terms are the threshold energies required for the processes of ionization, excitation, and elastic collision. The energies of the escaping ions and electrons and the plasma potential are

$$\varepsilon_i = \frac{T_e}{2} + |\Phi|, \qquad \varepsilon_e = 2T_e. \quad (28)$$

In this study, an input power modulated by an ideal rectangular waveform is used:

$$P_{abs}(t) = \begin{cases} P_0 & 0 \le t < \alpha_d\tau \\ 0 & \alpha_d\tau \le t < \tau, \end{cases} \quad (29)$$

where α_d is the duty ratio and τ is the pulse period.

III. SCALING LAWS

Scaling relations between the plasma parameters and the control parameters can be estimated based on the global balance equations. We assume that (1) a steady state is reached, (2) the dominant mechanism of generating ions is direct ionization of molecules and atoms, (3) the dominant loss mechanism is diffusion loss to the wall, (4) in the electron energy balance, the collisional energy loss is dominant, and (5) $K_{iz2} \simeq K_{iz1}, K_{rec2} \simeq K_{rec1}$.

In a previous article [18], we derived scaling formulas relating the charged-particle densities to the control parameters and to some internal plasma parameters based on the assumptions above. We observed that the positive-ion density increased with pressure at low pressures, reached a maximum, and then decreased slightly. This behavior seemed to be related to a transition of the dominant loss mechanism of the charged particles in electronegative plasmas. At low pressures, the dominant loss of charged particles is due to diffusion (we call this range the ion-flux-loss-dominated region) while at medium or high pressures, the loss takes place mainly via volume recombination (the recombination-loss-dominated region). The increase in volume recombination causes the charged-particle density to decrease with pressure since the more charged particles a discharge produces, the more recombination it results in. The increase in recombination loss, along with the diffusion loss, causes the charged-particle density to decrease.

The scaling formula for the positive ions for the ion-flux-loss-dominated region is

$$[O_2^+] \propto p^y P_{abs}, (y > 0). \quad (30)$$

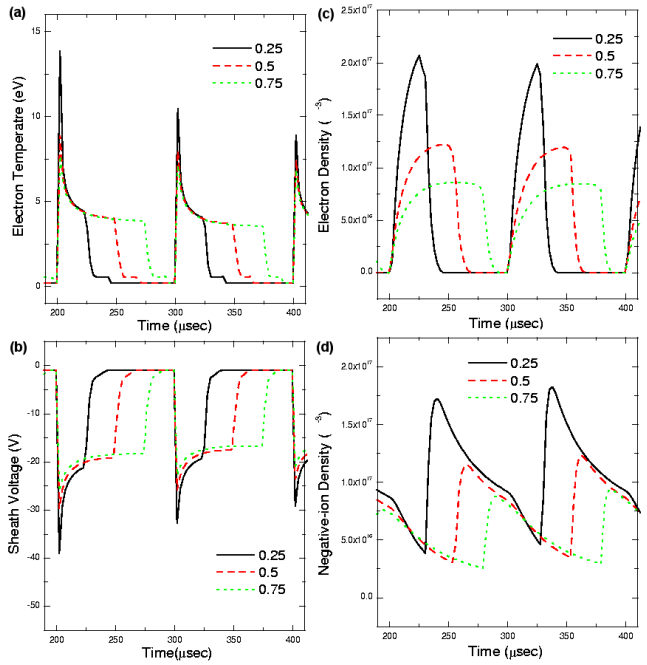

Fig. 1. Time-dependent (a) electron temperature, (b) sheath voltage, (c) electron density, and (d) negative-ion density in a pulse-modulated oxygen plasma for different duty ratios. The oxygen pressure was 20 mTorr, and the input power was 300 W.

Note that y depends on the gas composition, the operating region, and the chamber geometry. For the recombination-loss-dominated region, we have

$$[\mathrm{O}_2^+] \simeq [\mathrm{O}^-] \propto K_{iz2} P_{abs}^{1/2}. \tag{31}$$

Therefore, we notice that the positive-ion density decreases slightly with increasing pressure in this region since K_{iz2} decreases with pressure. This behavior was also observed in a pulsed oxygen discharge [27]. The simulation of Shibata *et al.* [29] showed a peak in the O_2^+ (dominant positive ion) density, and the experiment on a capacitively coupled oxygen discharge done by Stoffels *et al.* [30] showed a peak in the variation of the electron density with pressure.

A large O^+ concentration in a low-pressure discharge has been sought to obtain a well-defined implant depth for semiconductor and metallurgical applications. In a continuous high-density discharge, the efficient production of O^+ can be realized. It is known that the abundance of the atomic positive ion, O^+, depends on the surface recombination rate, the gas pressure, and the absorbed power. For a medium- or high-pressure discharge plasmas, O_2^+ is the major positive ion, and the oxygen molecules are far from being completely dissociated due to the very high oxygen-atom recombination frequency at the reactor walls. However, the degree of dissociation has been found to increase with the rf power. Lower pressure and higher power discharges have a larger atomic positive-ion density.

If we consider the representatively dominant reactions of generation and loss in Eq. (19), we have

$$K_{diss}[\mathrm{e}][\mathrm{O}_2] \simeq O_{Loss}[\mathrm{O}]. \tag{32}$$

From Eq. (24), we note $O_{Loss} = \gamma_{rec}/\tau_a$ ($\tau_a (= V/Av_{th})$ is the confinement time of the atom). Then, we can write

$$\frac{[\mathrm{O}]}{[\mathrm{O}_2]} \simeq \frac{[\mathrm{e}] K_{diss} \tau_a}{\gamma_{rec}}. \tag{33}$$

In a similar fashion, from Eq.(13) and Eq.(14),

$$O^+_{Loss}[\mathrm{O}^+] \simeq K_{iz1}[\mathrm{O}][\mathrm{e}], \tag{34}$$

$$O^+_{2Loss}[\mathrm{O}_2^+] \simeq K_{iz2}[\mathrm{O}_2][\mathrm{e}]. \tag{35}$$

By noting $O^+_{2Loss} = 1/\tau_i$ ($\tau_i (= d_{eff}/u_B)$ is the confinement time of ions), we have

$$\frac{[\mathrm{O}^+]}{[\mathrm{O}_2^+]} \propto \frac{[\mathrm{e}] K_{diss} \tau_a}{\gamma_{rec}}, \tag{36}$$

where we have assumed that molecular ions and the atomic ions have the same confinement time.

The confinement times, τ_a and τ_i, are insensitive to the plasma conditions [31]. As pressure increases, the electron density and K_{diss} decrease. Therefore, the ratio $[\mathrm{O}]/[\mathrm{O}_2]$ decreases with pressure. Increasing the pressure results in lower fractional dissociation; on the other hand, increasing the power results in higher fractional dissociation because the electron density increases with power. We can notice that $[\mathrm{O}^+]/[\mathrm{O}_2{}^+]$ scales similarly as $[\mathrm{O}]/[\mathrm{O}_2]$.

From Ref. 18, we write the scaling formulae for the ratio of the negative-ion density to electron density as

$$\frac{[\mathrm{O}^-]}{[\mathrm{e}]} \simeq \frac{K_{att}[\mathrm{O}_2]}{K_{rec}[\mathrm{O}_2^+]}. \tag{37}$$

This ratio increases with pressure, but decreases with power due to the increase in $[\mathrm{O}_2^+]$ in the higher-power region.

The scaling relations above hold regardless of cw operation or pulsed operation and have proven to be in agreement with the experimental results of cw operations [32,33]. In this study, we checked the validity of these scaling relations for the pulsed case.

IV. RESULTS AND DISCUSSION

Using a simulation based on the global model equations presented in Section II, we investigate the effects of the duty ratio, the modulation frequency, the pressure, and the input power on the time evolution of the charged particle densities and the electron temperature. The simulation device was a cylinder with R= 15 cm and L= 7.5 cm.

The calculated characteristics of a pulse-modulated oxygen plasma are shown in Fig. 1 for several duty ratios.

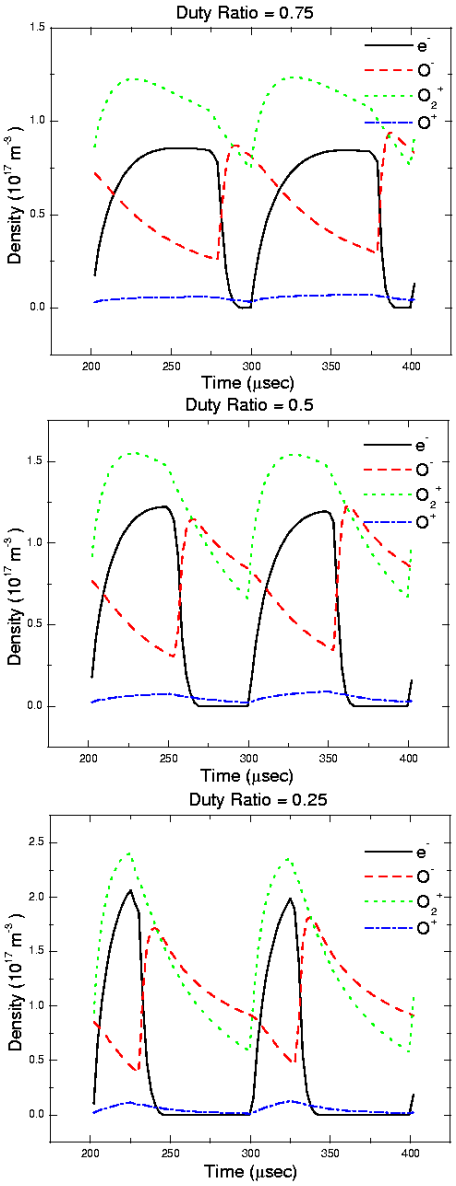

Fig. 2. Density of various species as a function of time for different duty ratios. The oxygen pressure was 20 mTorr, and the input power was 300 W.

The pressure was 20 mTorr at a 10-kHz pulse modulation frequency and a 300-W input power. We assume the O-atom recombiation coefficient at the wall to be 0.1.

A sharp overshoot at the first stage of the on-time is observed for the electron temperature and the sheath voltage profiles. This is attributed to the smaller number of electrons present at the first stage of power application. The peak electron temperature in a transient process is then higher at lower duty ratios. As the duty ratio increases, T_e approaches the value corresponding to cw operation. At all duty ratios, the electron temperature drops to insignificant values a few microseconds after the power is turned off. The characteristic decay time increases with the duty ratio.

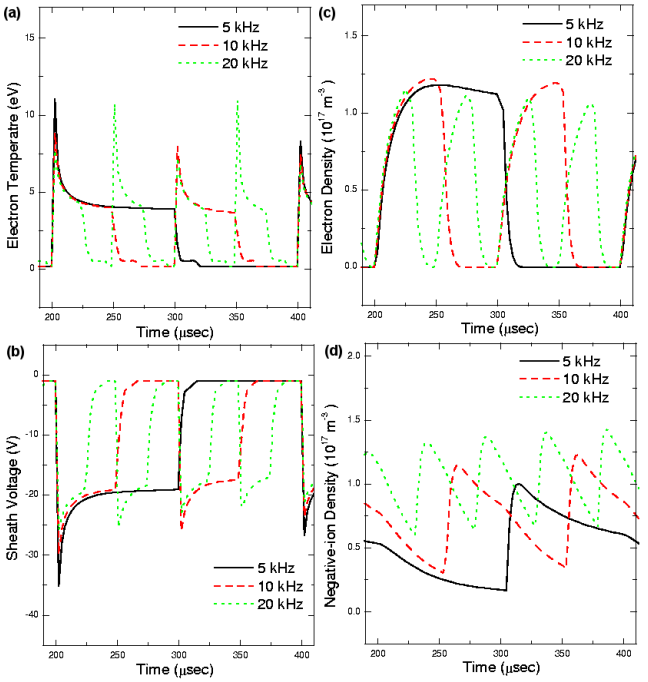

Fig. 3. Time-dependent (a) electron temperature, (b) sheath voltage, (c) electron density, and (d) negative-ion density in a pulse-modulated oxygen plasma for different modulation frequencies (duty ratio 50 %). The oxygen pressure was 20 mTorr, and the input power was 300 W.

The peak in the electron density increases as the duty ratio decreases, which is due to the increase in T_e associated with higher power during the discharge on time. This was observed experimentally by Ashida *et al.* [12]. The behavior of the sheath voltage is similar to that of the electron temperature.

When the power is turned on, the O^- density starts decreasing because of dissociation of molecular species that produce negative ions. When the rf pulse is turned off, the electron temperature plummets in the afterglow, and the attachment rate increases by several orders of magnitude. As a result, there is a large increase in the O^- density. However, at some point in the afterglow, the electron density decays sufficiently, and the O^- production rate begins to decrease. We note that the negative-ion density (peak and time average) increases with decreasing duty ratio due to the temperature dependence of the negative-ion creation and destruction reactions. The peak values of the density are larger than those for a cw plasma of the same average power. The increase in the plasma density is important for high processing rates. The offset of the period at which the negative-ion density start to rise depends on the duty ratio, and, for example it is about 50 μs for a duty ratio of 50 %.

It is possible to extract O^- out of the bulk plasma by modulating the plasma because the sheath voltage confines the negative ions as long as the power is applied. The negative-ion generation shows a maximum at a pe-

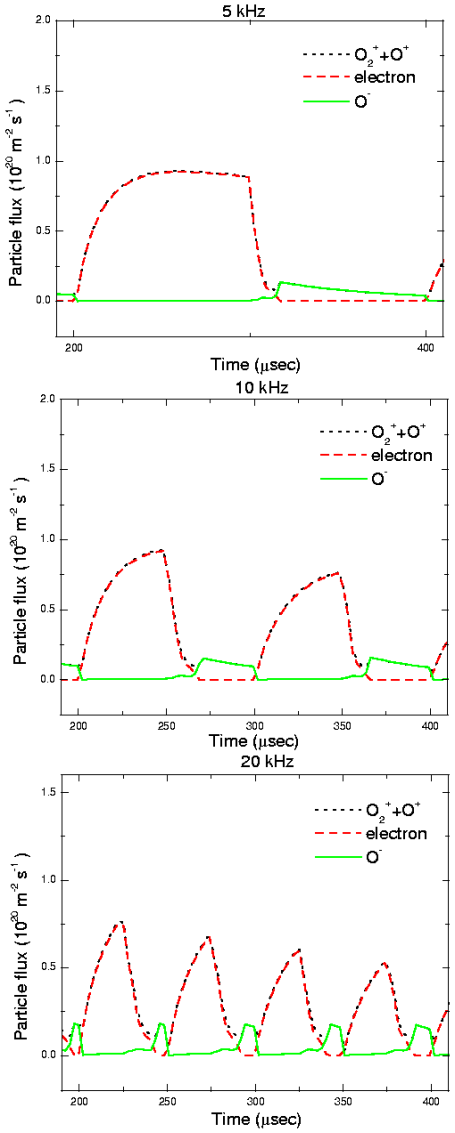

Fig. 4. Flux of various species to the wall as a function of time for different modulation frequencies. The oxygen pressure was 20 mTorr, the duty ratio was 50 %, and the input power was 300 W.

riod of about 60 μs for a duty ratio of 50 %. This is the same trend as in an argon plasma and a chlorine plasma. It should be noted that the densities of negative ions and electrons are strongly affected by the surface recombination coefficient, $\gamma_{\rm rec}$. The recombination coefficient for oxygen atoms at the wall plays an important role in determining the electronegativity of the plasma since the dissociative attachment fraction of the gas greatly affects the generation of negative ions.

Figure 2 shows charged-species densities during two periods for three different duty ratios. The electron and the positive-ion densities increase during the on-time of the pulse. Especially, they reach a maximum just when the power is turned off and continue to decline during

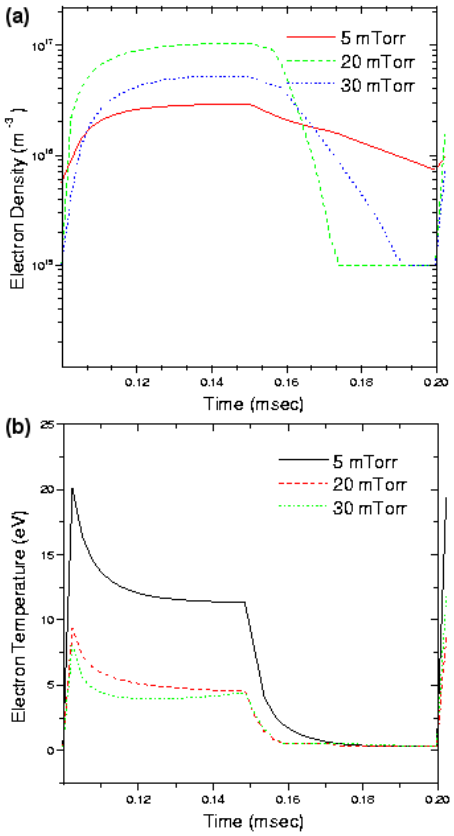

Fig. 5. Time-dependent (a) electron density, and (b) electron temperature for different pressures. The input power was 100 W, and the modulation frequency was 10 kHz.

the off-time in the case of a duty ratio of 0.25. We observe that just after the power has been turned off, the electron density decays faster than the positive-ion density. The relative densities of electrons, $O^+, {O_2}^+$, and O^- are strong functions of the degree of dissociation of molecular oxygen. This, in turn, strongly depends on the probability of recombination of atomic O into O_2 at the chamber walls. It is known that the O^+ yield increases with increasing electron density and that the O^+ density can be larger than the O_2^+ density in the high-power case [31]. For low or medium input power, a discharge has a low level of dissociation. Therefore, the O^+ density is quite small compared to the O_2^+ density.

Figure 3 shows the time-resolved plasma parameters for modulation frequencies of 5 kHz, 10 kHz, and 20 kHz. At a low modulation frequency (5 kHz), the plateau electron temperature is lower, and the negative-ion density becomes smaller. However, the time-averaged electron density gets slightly larger. The peak value of the negative-ion density increases with the modulation frequency.

Figure 4 shows the time evolutions of particle fluxes to the wall for different modulation frequencies. The negative ion flux to a wall in contact with the glow discharge is usually quite small because of the sheaths.

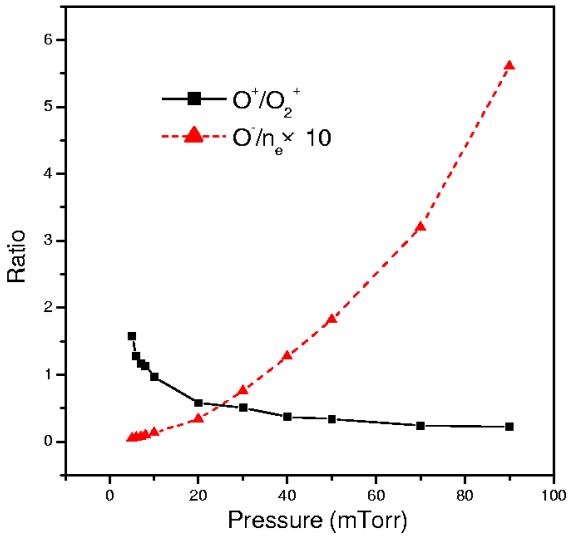

Fig. 6. Ratios O^+/O_2^+ and O^-/n_e as functions of pressure in the steady-state case. The input power was 1000 W, and $\gamma_{rec} = 0.1$.

In the afterglow, the sheaths decay on the time scale of the electron density loss rate while negative ions remain in the discharge region significantly longer. Therefore, the negative-ion flux to a wall can rise by a very large amount in the afterglow when the sheaths have diminished. This figure shows that the negative-ion flux reaches a maximum after the sheath fields have decayed to near zero. The peak value of the negative-ion flux gets larger slightly with increasing modulation frequency. This dependence was investigated experimentally by Overzet *et al.* [6] for a fluorine-helium discharge. They observed that the negative-ion flux increased with the modulation frequency up to a certain point and then decreased again (that is, had a maximum with respect to the modulation frequency). Time modulation can be effective because the negative-ion flux can neutralize the charge built up on a patterned surface. Samukawa and Ohtake [34] observed highly selective, highly anisotropic, notch-free, and damage-free poly silicon etching by using a chlorine gas in pulsed ECR plasmas. Pulsed operation supresses the accumulated charge in the feature.

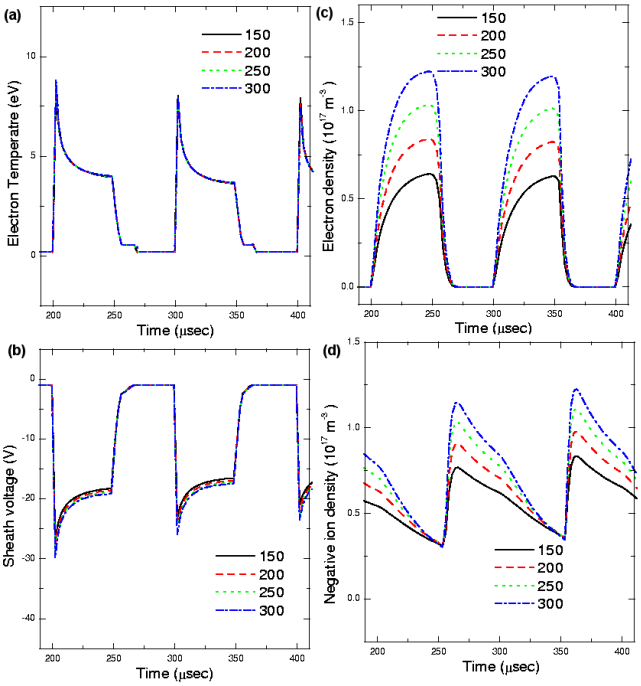

Fig. 7. Time-dependent (a) electron temperature, (b) sheath voltage, (c) electron density, and (d) negative-ion density in a pulse-modulated oxygen plasma for different input powers. The oxygen pressure was 20 mTorr, and the modulation frequency was 10 kHz.

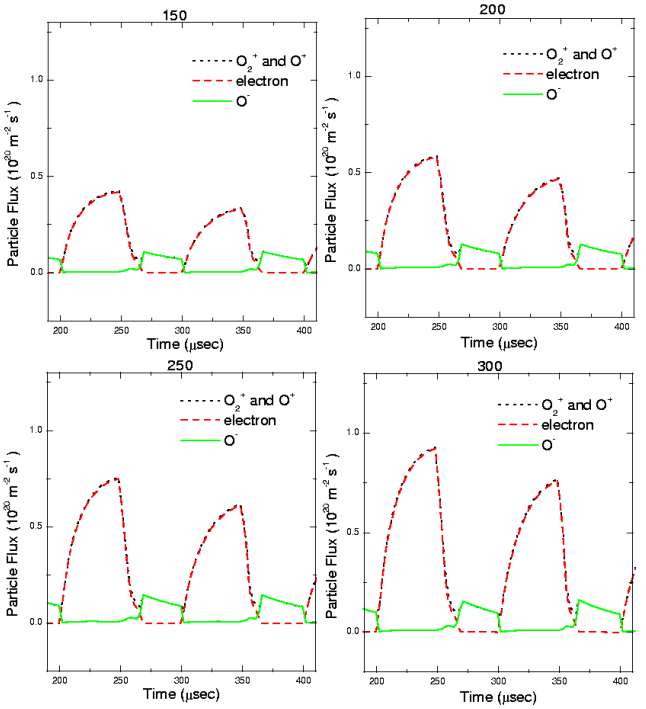

Fig. 8. Flux of various species to the wall as a function of time for different input powers. The oxygen pressure was 20 mTorr, and the modulation frequency was 10 kHz.

Figures 5(a) and 5(b) show the time-evolved electron density and electron temperature for pressures of 5, 20, and 30 mTorr. As is explained in the preceding section, the peak electron density has a maximum with respect to pressure. In this figure, the 20-mTorr case produces the largest peak density. This behavior was seen experimentally in a cw discharge [18,33], and theoretically by Panda *et al.* [27]. A decrease in electron temperature with pressure is a common phenomenon both in the cw case and the pulsed case.

Figure 6 shows the ratios O^+/O_2^+ and O^-/n_e for a steady-state cw discharge as functions of pressure. From the figure, we observe that the ratios are in good agree-

ment with the scaling formulas, Eqs. (36) and (37). Although not shown in the figures, the power dependences of O^+/O_2^+ and O^-/n_e were also examined and it was found that O^+/O_2^+ increased with increasing power whereas O^-/n_e decreased. The results agrees well with the experimental observations [35].

Figure 7 shows the effect of the input power on the time evolutions of the plasma parameters. The electron temperature and the sheath voltage have little dependence on the input power. However, at higher input power, the electron density and the negative-ion density become larger. This behavior is consistent with the scaling formulas derived based on global balance [18,36,37] and has been verified experimentally [38]. During the on-period, the electronegativity decreases with the input power, exhibiting a scaling similar to that for the cw case.

Figure 8 shows the particle flux to the wall for different input powers. The negative ion flux increases with the input power, but the slope of the increase is not as large as those of the electron density and the postive-charge density.

V. CONCLUSION

A spatially averaged (global) model, consisting of global particle and energy conservation equations, has been used to examine the characteristics of pulse-power-modulated oxygen discharges. The time-resolved characteristics of oxygen plasmas are investigated for various duty ratios, modulation frequencys, pressures and input powers. The characteristic decay time increases with the duty ratio. The peak in the electron density increases as the duty cycle decreases, which is due to the increase in T_e associated with higher power during the discharge on-time. The behavior of the sheath voltage is similar to that of the electron temperature. The peak negative-ion density in the afterglow increases with modulation frequency and input power, decreases with duty ratio, and shows a maximum with pressure. The pulsed discharge shows a pressure dependence similar to that of a cw discharge. Mass analysis, such as quadrupole mass spectrometry, is needed to investigate the scaling relations in the discharge in a more detailed manner. Pulsed-operation experiments are being performed to verify these scalings more precisely and to explore the scaling relations in broader operating regions.

ACKNOWLEDGMENTS

This work is supported by Korea Research Foundation (Grant No. 1999-015-DP0089) and by Hanbit User Program of the Korea Basic Science Institute.

REFERENCES

[1] St. Behle, A. Brockhaus and J. Engemann, Plasma Sources Sci. Technol. **9**, 57 (2000).
[2] S. Samukawa and S. Furoya, Appl. Phys. Lett. **63**, 2044 (1993).
[3] Y. Watanabe, M. Shiratani, Y. Kubo, I. Ogawa and S. Ogi, Appl. Phys. Lett. **53**, 1263 (1988).
[4] A. A. Howling, L. Sansonnens, J. L. Dorier and C. Hollinstein, J. Appl. Phys. **75**, 1340 (1994).
[5] M. B. Hopkins and K. N. Mellon, Phys. Rev. Lett. **67**, 449 (1991).
[6] L. J. Overzet, J. H. Bederman and J. T. Verdeyen, J. Appl. Phys. **66**, 1622 (1989).
[7] J. P. Booth and N. Sadeghi, J. Appl. Phys. **70**, 611 (1991).
[8] Y. Wang, E. C. Benck, M. Misakian, M. Edamura and J. K. Olthoff, J. Appl. Phys. **87**, 2114 (2000).
[9] A. Kono, M. Haverlag, G. M. Kroesen and F. J. De Hoog, J. Appl. Phys. **70**, 2939 (1991).
[10] X. Tang and D. M. Manos, Plasma Sources Sci. Technol. **8**, 594 (1999).
[11] M. V. Malyshev, V. M. Donnelly, J. I. Colonell and S. Samukawa, J. Appl. Phys. **86**, 4813 (1999).
[12] S. Ashida, C. Lee and M. A. Lieberman, J. Vac. Sci. Technol. A **13**, 2498 (1995).
[13] C. Lee and M. A. Lieberman, J. Vac. Sci. Technol. A **13**, 368 (1995).
[14] C. Lee, D. B. Graves, M. A. Lieberman and D. W. Hess, J. Electrochem. Soc. **141**, 1546 (1994).
[15] Y. T. Lee, M. A. Lieberman, A. J. Lichtenberg, F. Bose, H. Baltes and R. Patrick, J. Vac. Sci. Technol. A **15**, 113 (1997).
[16] M. A. Lieberman and S. Ashida, Plasma Sources Sci. Technol. **5**, 145 (1996).
[17] M. Yoon, S. C. Kim, H. J. Lee and J. K. Lee, J. Korean Phys. Soc. **32**, 635 (1998).
[18] T. H. Chung, H. J. Yoon and D. C. Seo, J. Appl. Phys. **86**, 3536 (1999).
[19] M. Meyyapan, J. Vac. Sci. Technol. A **14**, 2122 (1996).
[20] S. Ashida and M. A. Lieberman, Jpn. J. Appl. Phys. **36**, 854 (1997).
[21] M. Meyyapan, Jpn. J. Appl. Phys., Part I **36**, 4820 (1997).
[22] D. P. Lymberopoulos, V. I. Kolobov and D. J. Economou, J. Vac. Sci. Technol. A **16**, 564 (1998).
[23] V. Midha and D. J. Economou, Plasma Sources Sci. Technol. **9**, 256 (2000).
[24] R. W. Boswell and D. Vender, IEEE Trans. Plasma Sci. **19**, 141 (1991).
[25] D. Vender, H. B. Smith and R. W. Boswell, J. Appl. Phys. **80**, 4292 (1996).
[26] J. Mostaghimi, K. C. Paul and T. Sakuta, J. Appl. Phys. **83**, 1898 (1998).
[27] S. Panda, D. J. Economou and M. Meyyappan, J. Appl. Phys. **87**, 8323 (2000).
[28] B. Elliasson and U. Kogelschatz, *Basic Data for Modeling of Electrical Discharges in Gases: Oxygen*, KLR 86-11 C. (1986).
[29] M. Shibata, N. Nakano and T. Makabe, J. Appl. Phys. **80**, 6142 (1996).

[30] E. Stoffels, W. W. Stoffels, D. Vender, M. Kando, G. M. W. Kroesen and F. J. de Hoog, Phys. Rev. E **51**, 2425 (1995).
[31] T. Mieno, T. Kamo, D. Hayashi, T. Shoji and K. Kadota, Appl. Phys. Lett. **69**, 617 (1996).
[32] T. H. Chung, D. C. Seo, G. H. Kim and J. S. Kim, to apprear IEEE Trans. Plasma Sci., Oct. (2001).
[33] D. C. Seo, T. H. Chung, H. J. Yoon and G. H. Kim, J. Appl. Phys. **89**, 4218 (2001).
[34] S. Samukawa and H. Ohtake, J. Vac. Sci. Technol. A **14**, 3049 (1996).
[35] M. Tuszewski, J. Appl. Phys. **79**, 8967 (1996).
[36] A. J. Lichtenberg, M. A. Lieberman, I. G. Kouznetsov and T. H. Chung, Plasma Sources Sci. Technol. **9**, 45 (2000).
[37] T. H. Chung, J. Korean Phys. Soc. **34**, 24 (1999).
[38] D. Hayashi and K. Kadota, J. Appl. Phys. **83**, 697 (1998).